State-Space Modelling of Slow-Memory Effects Based on Multisine Vector Measurements[1]

Dominique Schreurs, Kate A. Remley*, Maciej Myslinski, Raf Vandersmissen**

K.U.Leuven, Div. ESAT-TELEMIC, Kasteelpark Arenberg 10, B-3001 Leuven, Belgium
E-mail: Dominique.Schreurs@esat.kuleuven.ac.be
*National Institute of Standards and Technology, 325 Broadway, Boulder, CO 80305, USA
**IMEC, Div. MCP, Kapeldreef 75, B-3001 Leuven, Belgium

Abstract

Non-linear microwave devices and circuits often exhibit slow-memory effects. When subjected to two-tone, or more general multisine excitations, the characteristics of these devices and circuits depend on the offset frequency between the tones. Since modulated excitations are an integral part of telecommunication systems, models aimed for circuit and system design should be able to accurately represent slow-memory behaviour. In this work, we develop a modelling procedure based on the state-space modelling approach to accurately incorporate these slow-memory effects. The technique is experimentally demonstrated on a High Electron Mobility Transistor (HEMT).

I. INTRODUCTION

Modulation schemes in current and future telecommunication systems become ever more complex, including a tendency toward broad modulation bandwidths. As a result, the classical approach to build non-linear models for microwave devices from single-tone small- or large-signal measurements is no longer always adequate. One reason for this is that single-tone microwave measurements cannot reveal slow-memory effects. Slow-memory effects occur when the device exhibits a frequency-dependent behaviour in the kHz-MHz frequency range that coincides with the usual range of baseband frequencies in modulated signals. Multiple physical causes may be present: thermal heating, trapping effects, impact ionization, baseband load impedance, etc. [1-4]. These slow, also called long-term, memory effects are often visualised by performing multitone measurements at varying offset frequencies, and by subsequently plotting the intermodulation product levels. If there is a dependency on the offset frequency, it indicates that phenomena giving cause to slow-memory effects are present in the device-under-test.

Ways to incorporate slow-memory effects in non-linear device models have already been presented in the literature [5-9]. Whereas most reported methods are related to the Volterra theory, our approach is based on an alternative technique, namely state-space modelling [10]. Furthermore, our method differs from related publications in that it is based on multisine measurements that are taken by a large-signal vector measurement system. Finally, our method is not limited to the modelling of components that have bandpass characteristics. In other words our approach does not suppose that higher order harmonics are filtered out.

In Section II, we describe the mathematical background and the practical implementation of the modelling procedure. In Section III, we present results of a simulation-based model for a MOSFET, and of a measurement-based model for a HEMT. Finally, conclusions are drawn in Section IV.

[1] *Work partially supported by an agency of the U.S. government.*

II. State-Space Modelling Including Memory Effects

A. Modelling Formalism

This work can be considered as an extension to our earlier developed state-space modelling approach [10]. This method involves representation of a microwave two-port device using equations of the form:

$$I_1(t) = f_a\left(V_1(t), V_2(t), \dot{V}_1(t), \dot{V}_2(t), \ddot{V}_1(t), \cdots, \dot{I}_1(t), \dot{I}_2(t)\right) \tag{1}$$

$$I_2(t) = f_b\left(V_1(t), V_2(t), \dot{V}_1(t), \dot{V}_2(t), \ddot{V}_1(t), \cdots, \dot{I}_1(t), \dot{I}_2(t)\right) \tag{2}$$

with $I_i(t)$ the terminal currents, and $V_i(t)$ the terminal voltages. The superscript dots denote (higher-order) time derivatives. This formalism does not incorporate slow-memory effects. It describes device current sources by representing the terminal currents as a function of the terminal voltages. The dependency on the first order voltage derivatives means that charge sources (or in the small-signal sense: capacitors) are also present in the device. Including higher order derivatives of the voltages and derivatives of the currents indicates the presence of RC-series connections, non-linear inductors, etc.

As the notion of derivative is related to the concept of time delay, equations (1)-(2) could be rewritten as:

$$I_1(t) = f_a\left(V_1(t), V_2(t), V_1(t-\tau_{rf}), V_2(t-\tau_{rf}), \cdots, V_1(t-n\tau_{rf}), V_2(t-n'\tau_{rf})\right) \tag{3}$$

$$I_2(t) = f_b\left(V_1(t), V_2(t), V_1(t-\tau_{rf}), V_2(t-\tau_{rf}), \cdots, V_1(t-n\tau_{rf}), V_2(t-n'\tau_{rf})\right) \tag{4}$$

with τ_{rf} a time-constant on the order of nanoseconds, which corresponds to behaviour at gigahertz frequencies, and n and n' being integer numbers to represent the equivalent of higher-order time derivatives. The higher order derivatives of the currents have been omitted, because non-linear inductive behaviour is rare in microwave components.

Slow-memory effects could be treated in a similar way. Slow-memory effects mean that the device characteristics are changing over the kHz-MHz frequency ranges, which corresponds to time-constants on the order of magnitude of milliseconds or microseconds. The consequence is that currents are not only dependent on what happened nanoseconds earlier (due to the fast-memory effects), but also milliseconds or microseconds earlier. The modelling equations subsequently become:

$$I_1(t) = f_a\left(V_1(t), V_2(t), V_1(t-\tau_{rf}), V_2(t-\tau_{rf}), \cdots, V_1(t-n\tau_{rf}), V_2(t-n'\tau_{rf}), V_1(t-\tau_{if}), V_2(t-\tau_{if}), \cdots, V_1(t-m\tau_{if}), V_2(t-m'\tau_{if})\right) \tag{5}$$

$$I_2(t) = f_b\left(V_1(t), V_2(t), V_1(t-\tau_{rf}), V_2(t-\tau_{rf}), \cdots, V_1(t-n\tau_{rf}), V_2(t-n'\tau_{rf}), V_1(t-\tau_{if}), V_2(t-\tau_{if}), \cdots, V_1(t-m\tau_{if}), V_2(t-m'\tau_{if})\right) \tag{6}$$

with τ_{if} the millisecond to microsecond level time delay, and n, n', m and m' being integer numbers.

As alternative representation, we could also express the scattered travelling voltage waves b_i (with subscript i the port index) in terms of the incident travelling voltage waves a_i, because the 'a/b' representation is analytically directly related to the 'v/i' representation. Consequently, equations (5)-(6) become:

$$b_1(t) = f_1\left(a_1(t), a_2(t), a_1(t-\tau_{rf}), a_2(t-\tau_{rf}), \cdots, a_1(t-n\tau_{rf}), a_2(t-n'\tau_{rf}), a_1(t-\tau_{if}), a_2(t-\tau_{if}), \cdots, a_1(t-m\tau_{if}), a_2(t-m'\tau_{if})\right) \tag{7}$$

$$b_2(t) = f_2\left(a_1(t), a_2(t), a_1(t-\tau_{rf}), a_2(t-\tau_{rf}), \cdots, a_1(t-n\tau_{rf}), a_2(t-n'\tau_{rf}), a_1(t-\tau_{if}), a_2(t-\tau_{if}), \cdots, a_1(t-m\tau_{if}), a_2(t-m'\tau_{if})\right) \tag{8}$$

In the next subsection, we discuss the procedure to identify these functional relationships for a particular microwave device.

B. Modelling Procedure

As we can see from equations (5) and (6), the method is based on time-domain data. These can be obtained from either simulations or measurements. Typically, simulations are performed on a circuit design consisting of several models for all constitutive active and passive components. Consequently, the goal of the behavioural modelling is to deduce a lower-order dynamic model that usually results in a significantly increased simulation speed. In the case of measurements, we opt to make use of large-signal vector measurements [11], because these systems provide calibrated measurements of both the amplitude and phase of the spectral components in a straightforward way. Calibrated measurements of both amplitude and phase are essential to deduce both short- and long-term memory effects. A limitation of our measurement set-up however is that no spectral components between DC and 600 MHz can be measured. As a consequence, only the intermodulation products around the carrier and those around the higher order harmonics of the carrier can be used in the modelling process.

As single-tone microwave measurements cannot reveal slow-memory effects, multisine measurements are essential to be able to characterise, and subsequently model, slow-memory effects. As our method is based on the time-domain representation, there is no theoretical restriction on the number of tones, although practical considerations, such as the maximum IF bandwidth of the measurement set-up, might impose an upper limit. In Ref. [12], we proposed use of a circuit-envelope procedure to efficiently make use of multisine-excitation-based measurements. In that work, we constructed behavioural models for devices with short-term memory effects. The principle that one multisine measurement can be converted into the equivalent of a set of single-tone measurements [12], can be utilized again here. However, the important addition is that the τ_{ij} time-delayed data also should be generated. This is accomplished by post-processing the measured data. Once all independent and dependent data are available, the functional relationships f_1 and f_2 can be determined. To accomplish this, we adopted an artificial neural network (ANN) representation based on one hidden layer and sigmoid activation functions. The training process uses the algorithm as developed by Ref. [13]. After training and testing the ANN, the model may be implemented in a microwave circuit simulator for further accuracy evaluation and eventual use in circuit and system design.

III. Modelling Results

We applied the modelling technique described above to two cases: First, we constructed a model from data obtained from simulations on a MOSFET transistor model with a low-frequency dependent behaviour. Secondly, we constructed a model from three-tone measurements on a HEMT transistor.

A. Simulation-Based Results

We first applied our proposed modelling approach to a simulated transistor model. The model is the empirical Chalmers model [14], implying that non-linear capacitors and current sources are represented by analytical expressions. The capacitance values are functions of the instantaneous voltages only. However, to simulate long-term memory effects, we deliberately introduced a frequency-dependence in the empirical expression for the drain current: the current varies between 30% of its nominal value at DC to 100% of its nominal value at 50 MHz. Simulations of the Chalmers model were then carried out using two-tone excitation at various offset frequencies. Consequently, an ANN was determined according to the formulas (7) and (8). Since the load during the simulation was exactly 50 ohms, it was sufficient to express the scattered travelling voltage waves b_1 and b_2 as functions of the instantaneous incident travelling voltage wave a_1, its first order derivative, and the τ_{ij} delayed parameter.

Figure 1 compares the original Chalmers model simulation ('x' symbols) to the results as simulated by the state-space model (circles). Denoting the two tones by f_{-1} and f_1, Figure 1 shows b_2 at f_1 and the third-order intermodulation product IM3 at the frequency $2f_1-f_{-1}$. We observe that the state-space model can

indeed predict a low-frequency-dependent behaviour. We notice that the agreement of both b_2 and IM3 is very good. This example demonstrates that the proposed method works in principle. A more realistic test on actual measurements is described in the next subsection.

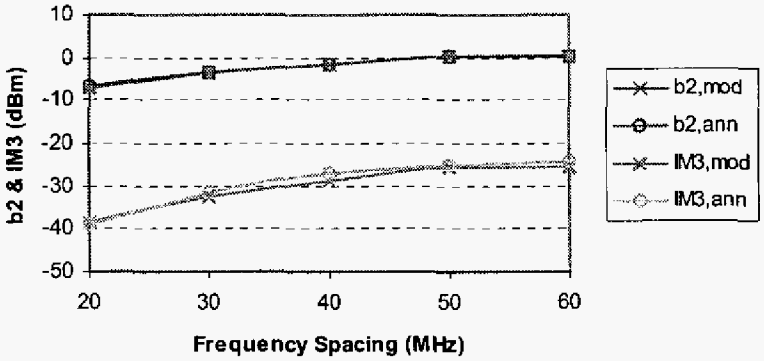

Figure 1: The 'x' symbols represent simulation results of an empirical model for an intrinsic MOSFET, where a low-frequency-dependent behaviour was deliberately introduced. The circles represent the results based on the state-space model. The top curve is b_2 at f_1, and the bottom curve is b_2 at the intermodulation product $2f_1$-f_{-1}. The carrier frequency is 800 MHz and the device is DC biased corresponding to maximum gain.

B. Measurement-Based Results

Before we collected measurements for model building, we first had to identify a device expected to exhibit slow-memory effects. We selected an on-wafer 0.15 µm x 100 µm GaAs based metamorphic HEMT (MHEMT). It is known that HEMTs, due to the difficult process of layer growth and device processing technology, are sensitive to the presence of traps. We anticipated that thermal heating and impact ionization would not be an issue with this particular device, due to the respectively small device width and the moderate DC bias. However, we expected that the IF impedance of the DC bias network might influence the device characteristics.

First, we performed two-tone, large-signal vector measurements [11] at various frequency offsets and RF input voltage amplitudes. Figure 2 shows the measured IM3 amplitude characteristic for the upper IM3 product. The variation in the amplitude characteristic with offset frequency clearly shows that slow-memory effects are present. The IM3 reaches a minimum around 10 kHz. Since the IM3 characteristic increases monotonically with applied voltage, we deduce that the memory effects do not depend on the input voltage level for these particular experimental conditions (fixed DC bias).

After this confirmation of the presence of slow-memory effects, we constructed a state-space model based on a three-tone, constant magnitude, constant phase excitation. The measurement set-up consisted of the large-signal vector measurement system, combined with an RF source that can generate multisine signals. For the model description, we again used the formalism of equations (7) and (8). Since there was no excitation at the drain side, a_2 only depended on possible mismatches, and therefore was small. Thus, we assumed that b_1 and b_2 were only dependent on the instantaneous voltage of a_2, and not on previous a_2 values, be it in the nanoseconds or milliseconds-to-microseconds range. Consequently, we expected that a good approximation for the HEMT was that the scattered travelling voltage waves were functions of the instantaneous values of a_1 and a_2, the first order derivative of a_1, and the τ_{if} delayed a_1. The results below will show that these approximations were justified. This consideration reduced the number of independent variables, which in turn reduced the ANN training time. In practice, a model envisaged for a circuit design should be accurate for a range of loads, implying a non-zero a_2. However, these simplified model expressions allowed us to prove the concept of the modelling procedure presented here.

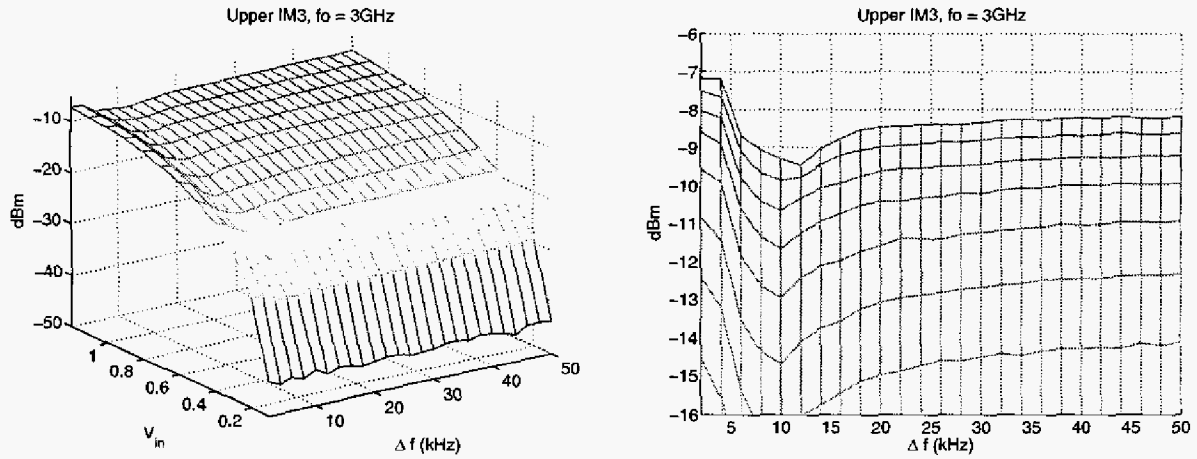

Figure 2: Measured IM3 as function of frequency spacing and RF input voltage amplitude (in [V]). The device is a GaAs MHEMT, biased for maximum gain. The right plot is a projection of the 3D-plot at the left to better visualise the frequency dependence of IM3 around 10 kHz.

Three-tone measurements were performed with the offset frequency between the three tones varied from 0.5 kHz to 87.5 kHz. More data were taken at smaller offset frequencies because of the larger IM3 variation across that range that we observed earlier. The amplitudes and phases of the three tones (denoted by the symbols f_{-1}, f_0, and f_1) were equal. From the measured data, we observed that b_1 was independent of the offset frequency, and consequently, no results concerning b_1 will be presented here. In Figure 3, we plot b_2 of tone f_1 (top curve), and the spectral component corresponding to $2f_1$-f_0 (bottom curve). The latter frequency component is similar to a classical third-order intermodulation product, although we do have interactions between three tones and not just two in this particular experimental example. The measurements are represented by the 'x' symbols in Figure 3.

After training the ANN and implementing the model in the microwave circuit simulator, the model was verified using envelope analysis. The simulation results are shown by means of circles on Figure 3. While the b_2 agreement at f_1 is excellent, there is still a small discrepancy between the IM3 measurements and simulations. Although errors can be introduced in all steps of the modelling procedure, we observed that especially the ANN training is a critical step.

As an independent check of the model accuracy, we excited the model with two other excitations. The first case (Fig. 4) utilizes a five-tone, constant magnitude, constant phase excitation with the same frequency offsets as used for the model construction (and thus a wider modulation bandwidth). The second case (Fig. 5) utilizes a two-tone excitation with frequency offsets different from the ones used during model construction. The amplitudes in both cases are chosen such that the (V_1,V_2) coverage areas are within the (V_1,V_2) coverage area of the state-space model. In both Figs. 4 and 5, we notice that the state-space model is able to represent the correct shape of the intermodulation product at $2f_2$-f_1 as a function of the frequency spacing. As well, the agreement for b_2 is excellent.

In conclusion, these verifications show that the modelling procedure, as described in Section II, can successfully be applied not only to simulation-based data (Section III.A.) but also to measured multisine, large-signal, vector data.

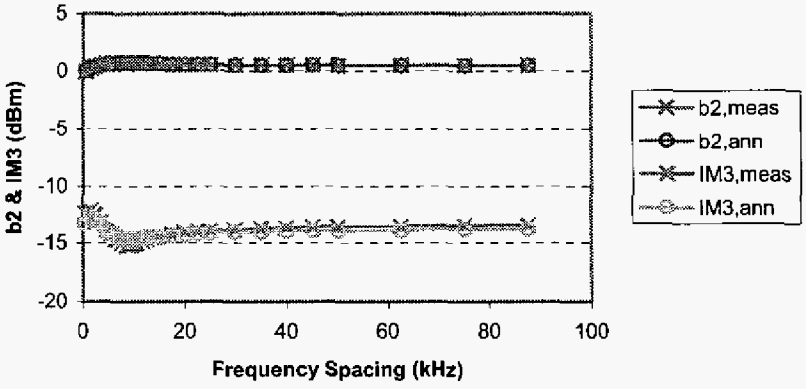

Figure 3: Measured ('x') and state-space model simulated (circles) b_2 at f_1 (top) and b_2 at $2f_1$-f_0 (bottom) for a three-tone, constant magnitude, constant phase excitation. The device is a HEMT, the carrier frequency is 3 GHz, and the device is DC biased to provide maximum gain.

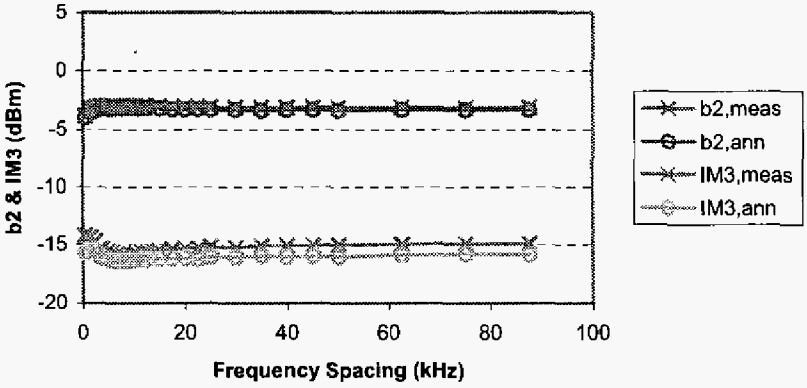

Figure 4: Measured ('x') and state-space model simulated (circles) b_2 at f_2 (top) and b_2 at $2f_2$-f_1 (bottom) in case of a five-tone excitation. The device is a HEMT, the carrier frequency is 3 GHz, and the device is DC biased to provide maximum gain.

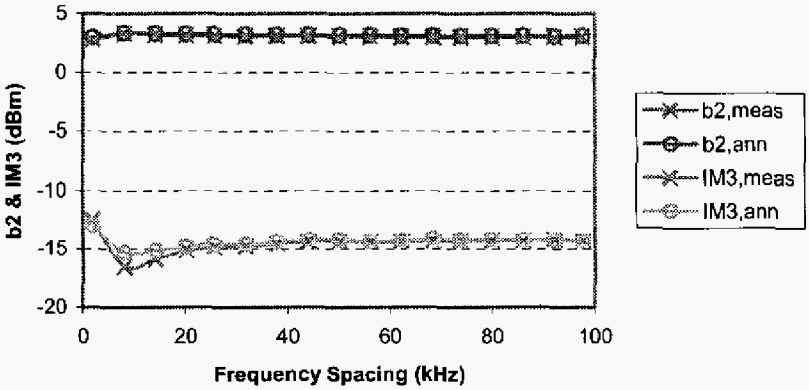

Figure 5: Measured ('x') and state-space model simulated (circles) b_2 at f_1 (top) and b_2 at $2f_1$-f_{-1} (bottom) in case of a two-tone excitation. The device is a HEMT, the carrier frequency is 3 GHz, and the device is DC biased for maximum gain.

IV. CONCLUSIONS

We described a way to incorporate slow-memory effects in the state-space modelling formulation. The principle is that the instantaneous terminal current values are functions of not only the state variables' values at a given point in time, but also of their values delayed with (a multiple of) the IF time constant τ_{if} and delayed with (a multiple of) the RF time constant τ_{rf}. The procedure has been verified, first on simulated data, and subsequently on measured large-signal data. We showed that this extended state-space model well predicts device behaviour even when the number of tones or the frequency offset of the multisine excitation is modified. This modelling approach will help circuit and system designers to better predict their designs' anticipated performance under modulated excitations.

ACKNOWLEDGEMENTS

D. Schreurs is supported by the Fund for Scientific Research-Flanders as a post-doctoral fellow. Div. ESAT-TELEMIC acknowledges F.W.O.-Vlaanderen for supporting this research. R. Vandersmissen acknowledges IWT.

REFERENCES

[1] A. Parker and J. Rathmell, "Measurement and characterization of HEMT dynamics," *IEEE Trans. Microwave Theory Techn.*, Vol. 49, No. 11, pp. 2105-2111, 2001.

[2] J. Vuolevi, T. Rahkonen, and J. Manninen, "Measurement technique for characterizing memory effects in RF power amplifiers," *IEEE Trans. Microwave Theory Techn.*, Vol. 49, No. 8, pp. 1383-1389, 2001.

[3] N. Borges de Carvalho and J.C. Pedro, "A comprehensive explanation of distortion sideband asymmetries," *IEEE Trans. Microwave Theory Techn.*, Vol. 50, No. 9, pp. 2090-2101, 2002.

[4] J. Brinkhoff and A. Parker, "Effect of baseband impedance on FET intermodulation," *IEEE Trans. Microwave Theory Techn.*, Vol. 51, No. 3, pp. 1045-1051, 2003.

[5] J.C. Pedro, N.B. Carvalho, and P.M. Lavrador, "Modeling nonlinear behavior of band-pass memoryless and dynamic systems," *IEEE International Microwave Symp.*, Philadelphia, PA, pp. 2133-2136, June 2003.

[6] H. Ku and J.S. Kenney, "Behavioral modeling of RF power amplifiers considering IMD and spectral regrowth asymmetries," *IEEE International Microwave Symp.*, Philadelphia, PA, pp. 799-802, June 2003.

[7] H. Ku, M. McKinley, and J. Kenney, "Extraction of accurate behavioral models for power amplifiers with memory effects using two-tone measurements," *IEEE International Microwave Symp.*, Seattle, WA, pp. 139-142, June 2002.

[8] T. Reveyrand, C. Maziere, J.-M. Nebus, R. Quere, A. Mallet, L. Lapierre, and J. Sombrin, "A calibrated time domain envelope measurement system for the behavioral modeling of power amplifiers," *Gallium Arsenide Application Symp.*, Milan, Italy, pp. 237-240, September 2002.

[9] T. Wang and T. Brazil, "The estimation of Volterra transfer functions with applications to RF power amplifier behavior evaluation for CDMA digital communication," *IEEE International Microwave Symp.*, Boston, MA, pp. 425-428, June 2000.

[10] D. Schreurs, J. Wood, N. Tufillaro, L. Barford, and D. E. Root, "Construction of behavioural models for microwave devices from time-domain large-signal measurements to speed-up high-level design simulations," *International Journal of RF and Microwave Computer Aided Engineering*, Vol. 13, No. 1, pp. 54-61, 2003.

[11] J. Verspecht, P. Debie, A. Barel, and L. Martens, "Accurate on wafer measurement of phase and amplitude of the spectral components of incident and scattered voltage waves at the signal ports of a nonlinear microwave device," *IEEE International Microwave Symp.*, Orlando, FL, pp. 1029-1032, 1995.

[12] D. Schreurs and K. Remley, "Use of Multisine Signals For Efficient Behavioural Modelling of RF Circuits with Short-Memory Effects," *Automatic RF Techniques Group Conf.*, Philadelphia, PA, pp. 65-72, June 2003.

[13] V. Devabhaktuni, M. Yagoub, and Q.-J. Zhang, "A robust algorithm for automatic development of neural-network models for microwave applications," *IEEE Trans. Microwave Theory Techn.*, Vol. 49, No. 12, pp. 2282-2291, 2001.

[14] I. Angelov, H. Zirath, and N. Rosman, "A new empirical nonlinear model for HEMT and MESFET devices," *IEEE Trans. Microwave Theory Techn.*, Vol. 40, No. 12, pp. 2258-2266, 1992.